The Co-Evolution of Post-Merger Galaxies and Dust-Reddened Quasars

Milena Crnogorčević

Department of Physics, Middlebury College, Middlebury, Vermont 05753

Project Report for PHYS0704

Abstract

This project utilizes data obtained from the OSIRIS integral field spectrograph combined with Laser Guide-Star Adaptive Optics (LGS) to better understand the evolution of moderately dust-reddened quasars as well as their hosting galaxies. The quasars considered are located in galaxies with high degree of merger activity, and thus we expect to see intense star-formation regions. The high spatial resolution of OSIRIS+LGS enables the analysis of the quasar contribution separately from that of star-formation regions. In turn, this provides more information about the host galaxy's activity. The goal is to characterize the evolutionary stage of the host galaxy by extracting information about the degree of star formation and the kinematics for five different targets.

Signatures

Advisor: _____
(E. Glikman)

2nd reader: _____
(J. Dunham)

Date accepted: _____

Acknowledgments

I gratefully acknowledge Professor Eilat Glikman for her constant guidance and willingness to impart knowledge about the universe, Jonathan Kemp, for his immense help with the OSIRIS pipeline installation and function, as well as the Middlebury College Department of Physics for this invaluable learning opportunity.

Contents

List of Figures

1 Introduction

1.1 Historical background

To the surprise of most astronomers of the time, many point-like optical counterparts to radio sources were detected in the early days of radio astronomy [1]. Initially, they were described as a new class of radio-loud stars in our Galaxy. Improvements in the instrumentation's precision allowed for more detailed observations. Emission spectra of the observed sources revealed broad emission lines at wavelengths uncharacteristic of a star, necessitating a revision of the previously proposed theory. In 1963, a Caltech astronomer Maarten Schmidt realized that broad emission lines in question correspond to red-shifted Balmer series of hydrogen energy transitions, resulting in a discovery of a new class of sky objects [2]. The discovery of quasi-stellar radio sources (quasars) provided further evidence for the expansion of the Universe, a key feature of the Big Bang cosmology, as well as revolutionized extragalactic astronomy. Following the first discovery, many new quasars were identified. Moreover, a great number of radio-quiet, but luminous, point-like objects were observed thereupon, further expanding the newly-formed class of sky objects. Radio-quiet high-luminosity stellar-appearing sources, or "quasistellar objects" (QSOs), are still commonly referred to by their firmly established misnomer – quasar. To the contrary of the initial view, it is now well-known that only 10% of all quasars are radio emitters [3]. Most quasars are observed at redshifts up to $z = 3.5$, but some of them are seen as far as $z = 7.1$ (ULAS J1120+0641) [4], representing the most distant objects observed in the universe [5]. Quasars' characterization is still a question of interest for many and is an active field of research.

1.2 Physical properties of a quasar

In the center of a massive galaxy resides a supermassive black hole (SMBH; $10^6 - 10^9 M_\odot$, where $M_\odot$ is the mass of the Sun) [6]. The gravitational potential of a black hole causes gas and dust particles to spiral towards its center, resulting in the formation of an accretion disk extending toward the event horizon. Rapidly moving particles in the inner regions of the accretion disk move faster than particles in the outer regions. The viscosity between different layers of matter in the accretion disk causes gravitational energy to be transformed into radiation. This compact region of strong light emission close to the event horizon is called an Active Galactic Nucleus (AGN). Due to temperature differences within the accretion disk, the emission spectrum of a quasar is a superposition of many blackbody curves, resulting in a power-law shape. Its spectrum is characterized by broad emission lines rising above a strong continuum, and sometimes absorption lines from the host galaxy. Atomic gas in the accretion disk rotates at a range of speeds, resulting in both a blueshift and a redshift of emission peaks, which causes their broadening. The compact continuum source, i.e., the accretion disk, is surrounded by an optically thick torus of molecular dust, which blocks a direct view of the active regions from certain viewing angles. The excitation of the cold tenuous gas far beyond this region, even extending into the host galaxy, results in a narrow-line emission [1, 5]. The most commonly accepted model that explains enormous energy output from an AGN, despite its comparably small size, is the accretion onto a SMBH [7].

Among AGNs, quasars are the most luminous, falling in the range between 10^{42} and 10^{48} erg/s (luminosity of the Sun $L_\odot = 4 \times 10^{33}$ erg/s). The luminosity of a quasar is given by a time derivative of Einstein's energy/mass equation,

$$L = \eta \dot{M} c^2, \tag{1.1}$$

where $\dot{M}$ is the accretion rate, and η is the efficiency of the conversion process of mass to radiant energy. To achieve such high orders of magnitude for the luminosity, the efficiency of the conversion process η must be high. For a quasar, η is on the order of 10^{-1}. As a comparison, the efficiency of a fusion bomb is approximately 0.003 [5]. On the other hand, the upper limit of

an object's luminosity fueled by accretion is determined by the Eddington luminosity limit,

$$L_{\text{edd}} = \frac{4\pi GcMm_p}{\sigma_T}, \tag{1.2}$$

where G is the gravitational constant, c is the speed of light, M is the mass of the black hole, m_p is the mass of a proton, and σ_T is the Thomson cross section. The Eddington limit is reached when the outward radiation pressure outbalances the inward gravitational pressure, thus not allowing any particles to accrete [5].

One way to fuel accretion onto a black hole is through merger activity. When two or more galaxies collide, their respective black holes merge into one SMBH. This collision is followed by a high concentration of particles with random kinetic energies. Initially, some of the particles fall into the new potential well, fueling the newly formed quasar. The rest is distributed around the accretion disk, scattering and absorbing the blue light emitted by the quasar, effectively decreasing the observed luminosity of the source. Such obscured sources fall under the category of dust-reddened quasars [8], and is assumed to be one of the first post-merger evolutionary stages of a galaxy [7].

1.3 Merger-induced star formation

Galaxy interactions and mergers can trigger the star formation process [9]. When two or more galaxies collide, gas particles from one galaxy are influenced by the gravitational pull from other galaxies. Initially, asymmetric superposition of multiple galaxies' gravitational fields causes a non-axisymmetric distribution of gas clouds. These gas clouds fall into denser gas regions due to gravitational torquing, resulting in a cloud's collapse under its own gravity. The collapse is followed by a formation of massive stars that fuse hydrogen and helium atoms into elements with higher atomic numbers, as well as a strong narrow line emission by photoionizing the surrounding gas that has not yet reached clouds [5]. Since the entire process takes place in proximity to the newly formed galaxy center, it is called a centralized or nuclear starburst. Hence, the model in [9] predicts an increased star formation rate during galaxy mergers within regions in the immediate surrounding of the black hole. To model the star formation process we

use the Schmidt law,

$$\frac{\mathrm{d}\rho_\star}{\mathrm{d}t} = C_\star \frac{\rho_{\mathrm{gas}}}{t_{\mathrm{dyn}}}, \tag{1.3}$$

where $\rho_\star$ is the stellar density, ρ_{gas} is the gas density, $C_\star$ is the star formation efficiency, and $t_{\mathrm{dyn}} = (\sqrt{4\pi G\rho_{\mathrm{gas}}})^{-1}$ is the local dynamical time [10].

Observational data of some galaxy mergers are in partial disagreement with the model described above [11]. In these observations it was found that some of the star-forming regions extend far beyond the central 100-1000 pc in diameter. Shock-induced star formation has been suggested to explain the spatial extension of the merger-induced star formation [5, 11].

Observing and obtaining emission spectra from merger-induced star formation regions is challenging, as it can be compromised by the extremely bright light from the quasar. To account for this challenge, we use an integral field spectrograph with an adaptive optics system to obtain the data for selected objects.

1.4 Co-evolution hypothesis

Hopkins et al. [7] establish a model in which a merger of gas-rich galaxies fuels both star formation, as well as black hole accretion, predicting a dust-reddened phase of a newly formed quasar. Furthermore, they show that dust-reddening of a quasar is anti-correlated with its age. At redshifts from 3 to 2, corresponding to a time when the universe was 2.171 Gyr to 3.316 Gyr old (16% to 24% of its current age) [12], the population of quasars is the highest. At the same evolutionary stage of the universe, the star formation rate density reaches the highest value as well, suggesting a link between the black hole's growth and the star formation rate. Figure 1.1 shows the timeline of the post-merger galaxy evolution. To thoroughly characterize a merger-driven formation of a galaxy, we simultaneously examine the extent of star-formation as well as the dust-reddened quasar's activity. We expect to see high levels of both aforementioned processes in these assembling systems [8].

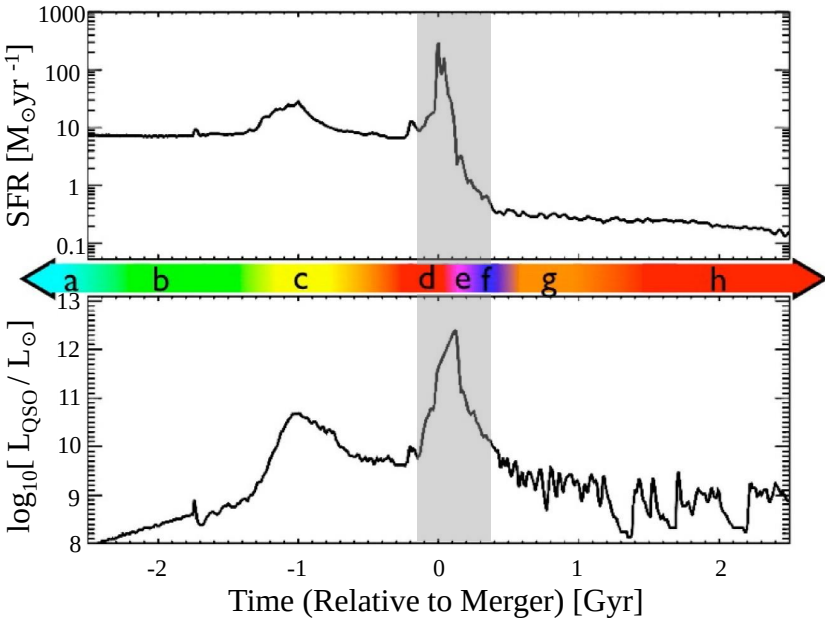

Fig. 1.1. Evolutionary stages of galaxy undergoing a gas-rich merger. The upper panel corresponds to the star-formation activity, with star-formation rate in $M_\odot$ per year on the vertical axis. The lower panel corresponds to the activity of the quasar in the same galaxy, with the quasar luminosity on the vertical axis. The horizontal axis shows time relative to the merger. Collision between two galaxies happens in (c), followed by strong star-formation rate and high quasar activity. We are examining systems in stage (d-f), highlighted in gray. After (e), the model predicts less activity, leading to a final evolutionary stage, or a "dead" elliptical shown in (h) [7].

2 Instrumentation

Moderately dust-reddened quasars believed to be in stages (d-f) in Fig. 1.1 were selected for observation using the OSIRIS Integral Field Spectrograph (IFS) with Keck Adaptive Optics System (AO). Due to a high rate of merger activity of targets in question, the high angular-resolution and spatially-resolved spectroscopy of the OSIRIS instrument is optimal for providing the information necessary to probe into quasar/galaxy co-evolution. Furthermore, all of the objects observed are brightest and least obscured in the infrared region, which corresponds to the range of wavelengths of OSIRIS's sensitivity.

2.1 OSIRIS

OSIRIS (OH-Suppressing InfraRed Integral-field Spectrograph) is a near-infrared integral-field spectrograph at the W. M. Keck Observatory that uses an array of lenses allowing the collection of spectra from up to 3000 locations simultaneously. The spectrograph is designed to operate within the near-infrared, ranging from 1 to 2.4 μm in wavelength. In the broad-band mode, each pixel in the 16×64 rectangular grid contains a 1700-pixel spectrum covering the entire range of the infrared broadbands (*z, J, H,* or *K*). In the narrow-band mode, the rectangular grid ranges from 16×64 to 48×64 pixels, depending on the filter used. The narrow-band provides a 400-pixel spectrum for each lenslet, only partially covering the infrared bands. The spectrograph uses four plate scales, 0.020, 0.035, 0.050, and 0.100 arcsec per lenslet. Thus, the field of view ranges from 0.32×1.28 arcsec^2 to 1.6×6.4 arcsec^2 for the broad-band mode, and from 0.32×1.28 arcsec^2 to 4.8×6.4 arcsec^2 for the narrow-band mode. For a comparison, the angular size of the Moon is 31 arcmin, which is approximately equivalent to the size of a thumbnail at arm's length. One arcsecond corresponds to the size of a thumbnail held at a distance of approximately 2 km.

Hence, the large amount of spectral data is confined to a very small field of view [13].

2.2 Keck Adaptive Optics System

To approach the resolution limit governed by diffraction

$$\theta = 2.5 \times 10^5 \frac{\lambda}{D}, \tag{2.1}$$

where θ is given in arcseconds, λ is the wavelength of the observed light in meters, and D is the diameter of telescope objective in meters, one must take into consideration the turbulence of air particles in the Earth's infrared-loud atmosphere [14]. The size of the seeing disk at W. M. Keck Observatory, Mauna Kea, is about 0.5 arcsec. Considering the OSIRIS's small field of view, the use of the Keck AO system to compensate for atmospheric turbulence is of crucial importance. AO uses a sensor to constantly monitor the atmospheric conditions and a deformable mirror to account for the incoming wavefront distortions. The sensors require a sufficient signal-to-noise ratio to measure the atmospheric variations, so a Natural Guide Star (NGS) or a Laser Guide Star (LGS) are used as a reference source. Figure 2.1 illustrates the resolution improvement when AO system is used. Finally, Fig. 2.2 illustrates the complete optical configuration of the OSIRIS with the Keck AO system.

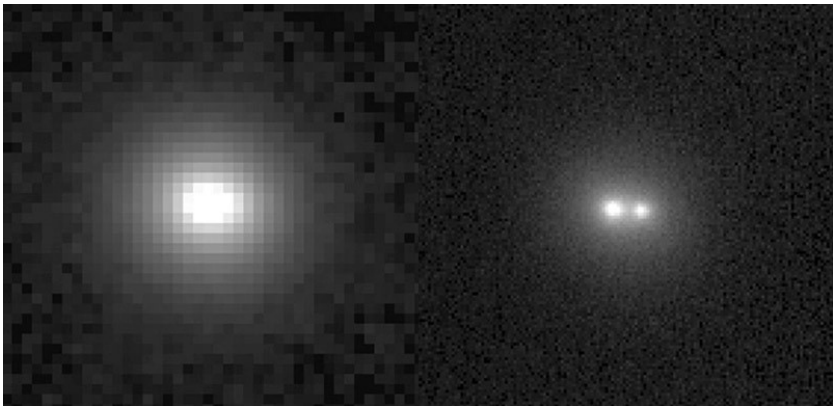

Fig. 2.1. Near-infrared image of a galaxy undergoing a merger, as seen without the Keck AO system (left), and with the Keck AO system (right). Credit: UCSC, UCLA, W. M. Keck Observatory

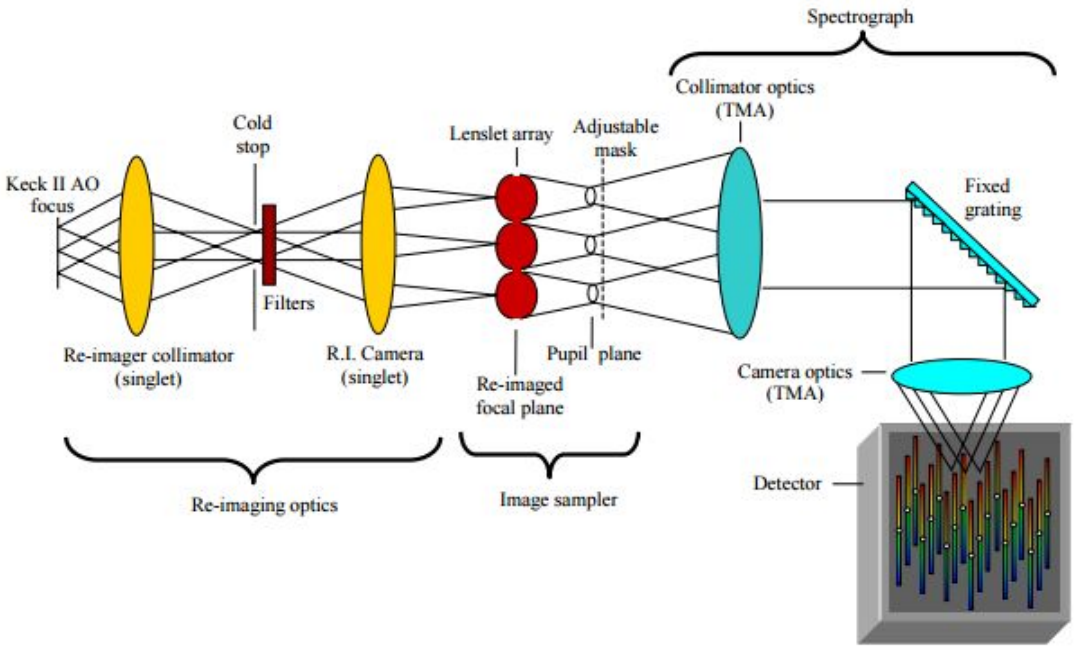

Fig. 2.2. A schematic of OSIRIS and the Keck AO optical configuration. Shown are three coupled systems: a re-imager, an image sampler, and a spectrograph. The re-imaging optics determines the spatial scale of the instrument. The image sampler consists of an array of lenslets that store pupil images of all the light coming from a certain position in space, that is then dispersed by the spectrograph and detected by the detector. The lenslet array is rotated by 3.6 degrees, preventing the spectra from overlapping. There are twenty three types of filters to select out different wavelength regions [13].

3 Data manipulation

The final integral field spectrum of objects is a three-dimensional data cube, with one dimension in wavelength space, and the other two showing position in the sky. Figure 3.1 illustrates the process required to obtain the final data cube.

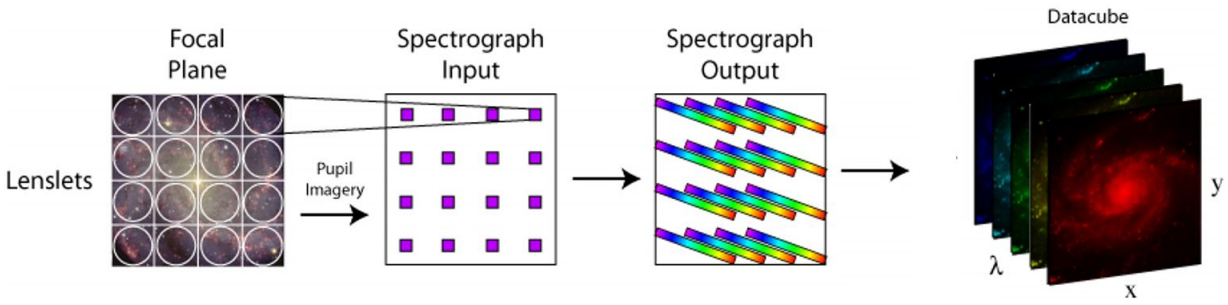

Fig. 3.1. Schematic showing the process required to obtain the final data cube. An array of lenslets transmits light from adjacent points in the sky, which is then dispersed by the spectrograph. The data collected is mosaicked into a single three-dimensional data cube with one spectral and two spatial axes. Adapted from [15].

3.1 Observation and data collection

Five moderately dust-reddened quasars were selected for observation using the OSIRIS with the Keck AO system. Hubble Space Telescope (HST) images of some of these quasars indicated that their host galaxies reveal a high degree of merging activity. Figure 3.2 shows Sloan Digital Sky Survey's (SDSS) images of the observed objects as seen in optical light. Table 3.1 lists all the targets with their identifying characteristic values.

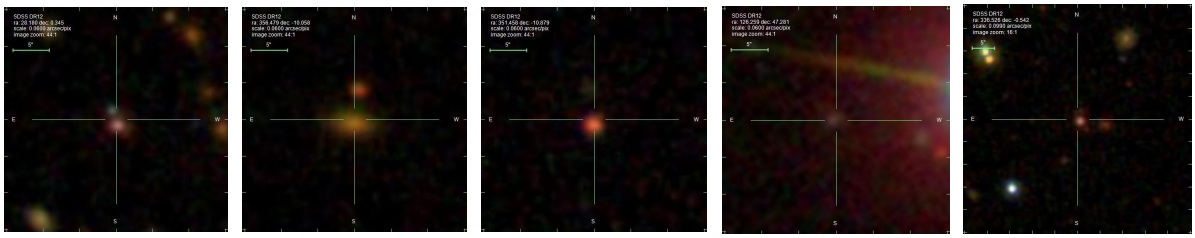

Fig. 3.2. Optical images of the sources observed, as reported by SDSS. Both axis show angular positions of the object in the sky. From left to right are arranged: UKFS0152+0020, F2345-1003, F2325-1052, F2M0825+4716, and S82M2226-0032. Credit: SDSS.

Table 3.1. Five targets selected for observation. Reported is a summary of their properties, including their position in the sky, redshift, K-magnitude, filter used throughout the observation, expected emission line, and the magnitude of their corresponding NGS [13].

Object	R.A.	Dec	Redshift, z	K (mag)	Filter	Line	NGS (mag)
UKFS0152+0020	01:52:43.18	+00:20:40.3	0.578	16.3	Kbb	Paβ	14.92
F2345-1003	23:45:54.91	-10:03:29.1	0.263	14.2	Hbb	Paβ	15.32
F2325-1052	23:25:49.89	-10:52:43.4	0.564	15.2	Kbb	Paβ	15.04
F2M0825+4716	08:25:02.04	+47:16:52.2	0.803	14.1	Zbb	Paβ	11.3
S82M2226-0032	22:26:06.22	-00:32:32.4	0.578	15.1	Kbb	Hα	15.5

3.2 Data reduction and OSIRIS pipeline

The OSIRIS data reduction pipeline is an Interactive Data Language (IDL) software designed to reduce the infrared data cube to enable further analysis. It accepts commands only from XML files (in OSIRIS literature referred to as Data Reduction Files or, DRFs), generated by the OSIRIS Graphic User Interface (GUI) or by hand. The pipeline is described in detail in [13] and [16] with a step-by-step users' manual included in both.

We obtained raw images at the telescope in the form of FITS files containing spectral information, with the spatial and filter details recorded in the header. The data reduction

process consists of subtracting dark and scaled sky frames, telluric correction, calibrating the wavelength scale, and mosaicking the data into one final data cube, done with the GUI and occasional use of IDL scripts.

Dark frames are images taken with the same exposure time as the target's images, but with no light collected. These calibrations measure the time-dependent charge buildup in the CCD that is not due to the incoming light from the object. The dark frames are combined into a super-dark frame, that is then subtracted from all subsequent images.

We observe a target by alternating between looking at the object itself and an empty region of the sky. As the sky is very bright in the infrared, it is crucial to remove any sky emission from our objects' images. We do so by scaling and subtracting the sky frame for every scientific frame at each wavelength.

For every filter used in our observations, we obtain several images of an A0-type star (NGS) to account for transmission variations of the atmosphere. For each quasar, we identify a near-by star located at an elevation and atmospheric conditions similar to that of our source. Extracting the telluric (atmospheric) standards consists of reducing the star frame and calibrating the wavelength. Data calibration is done by including a calibration file from the OSIRIS data base that corresponds to the filter and the plate scale used throughout the observation.

The final step is processing object frames from each set, and computing quasar centroid offsets. Finally, we mosaic all object frames into a single data cube, that enables spectral extraction necessary for the analysis.

4 Notes on individual objects

In this project, data of three objects were successfully reduced. These objects include F2M0825+4716, F2345-1003, and S82M2226-0032, leaving UKFS0152+0020 and F2325-1052 for future reduction and analysis. Reduction steps are described in detail in [13] and [16]. Figure 4.1 shows the final data cube for each source. The first part of the analysis for each reduced data cube involves approximating the observed linear size of the host galaxy l, given by

$$l = \frac{D_A \times \theta(\text{arcsec})}{206\ 265}, \tag{4.1}$$

where θ is the angular size of the object and D_A is the angular distance size reported in [12], assuming the current cosmological constants (Hubble constant H_0= 69.6 (km/s)/Mpc, matter density parameter Ω_m = 0.286, and vacuum density parameter Ω_Λ= 0.714). Furthermore, we fit Gaussian curves to sources' spectral intensities, allowing for the analysis of their symmetry properties through the consideration of FWHM values in both spatial directions. Finally, we analyze spectra collapsed over the spatial extent of each host galaxy, and identify elements corresponding to different emission lines we observe.

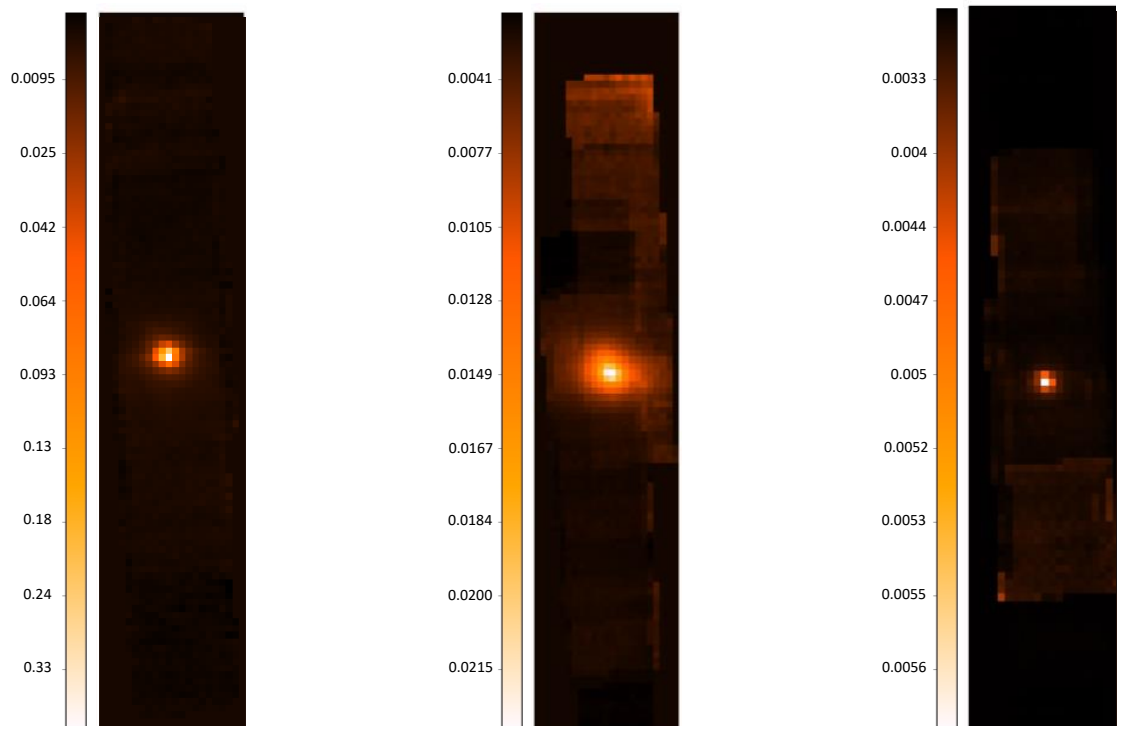

(a) F2M0825+4716 (b) F2345-1003 (c) S82M2226-0032

Fig. 4.1. Reduced three-dimensional data cubes. Shown is the object's position in the sky. The color gradient indicates the intensity at each pixel in arbitrary units. The brightest pixels represent the position of the quasar. Note the extended emission beyond the central source, likely from the host galaxy. Each pixel corresponds to 0.1×0.1 arcsec^2.

4.1 F2M0825+4716

Observations of F2M0825+4716 were conducted on November 5$^{\text{th}}$ and November 6$^{\text{th}}$, 2012. Reduction and spectral analysis of this source was previously reported in [16]. In this project, F2M0825+4716 was used as a reference to ensure that the reduction process described in [13] and [16] results in an equivalent final data cube, even though executed in a different version of the OSIRIS pipeline.

Among five objects observed, F2M0825+4716 is the one that is the farthest away, with a redshift of $z = 0.803$. The filter used for this observation is Kbb, allowing the wavelengths from 1965 nm to 2381 nm. [13] The Kbb transmission curve is shown in Fig. 4.2. The spatial scale

is 0.1 arcsec, allowing for 1.6×6.4 arcsec^2 field of view. The integration time is 600 s, totaling in 210 min of target observation, and 80 min of the sky observation. A total of 20 s is used to observe a NGS for the telluric (atmospheric) correction.

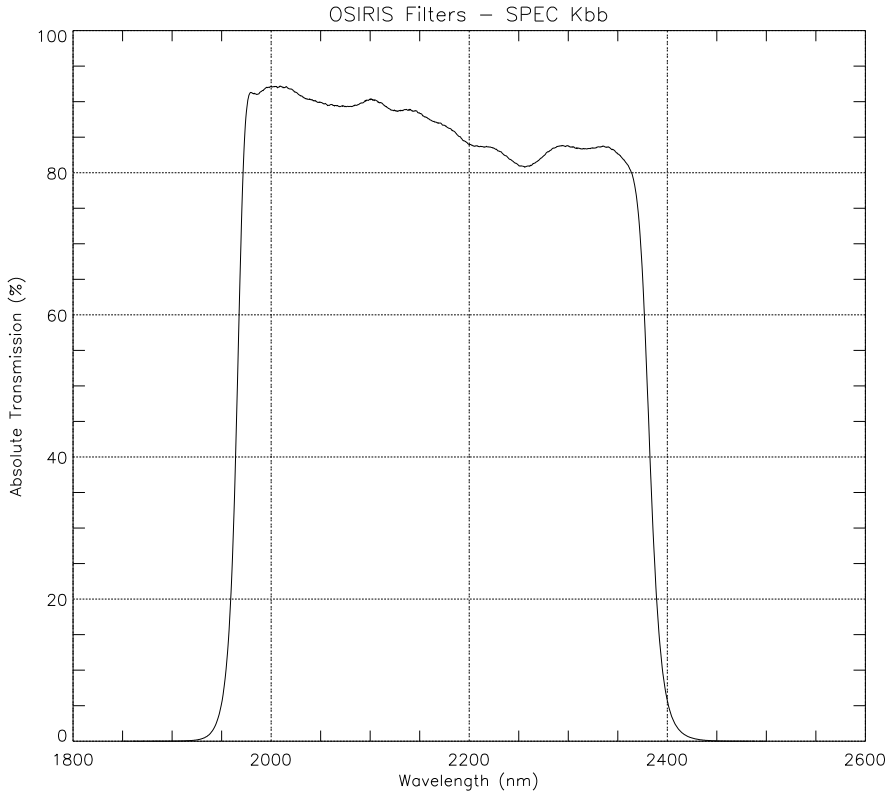

Fig. 4.2. Transmission curve for the OSIRIS Kbb filter, used for the observation of F2M0825+4716. Kbb is a K-band filter allowing the transmission range from 1965 nm to 2381 nm.

Object's frames are reduced and mosaicked into a single three-dimensional data cube shown in Fig. 4.1(a). Using the `Horizontal cut` function in Quicklook2 allows for approximation of the host galaxy's diameter. For F2M0825+4716, we find that the diameter is approximately 17 pixels, or $\theta = 1.7$ arcsec in angular size. Reference [12] reports that, under the current cosmological parameters for a source at $z = 0.801$, the angular size distance is $D_A = 1569.4$ Mpc. Substituting these values into Eq. (4.1), we find that the observed linear size of the host galaxy is 13 kpc. Furthermore, fitting a Gaussian curve to the source's spectral intensity results

in a FWHM of 1.56 pixels (∼1.19 kpc) in the horizontal direction, and 1.54 pixels (∼1.17 kpc), suggesting a symmetric source, which might suggest a lack of merger activity, though optical images from the HST suggest otherwise.

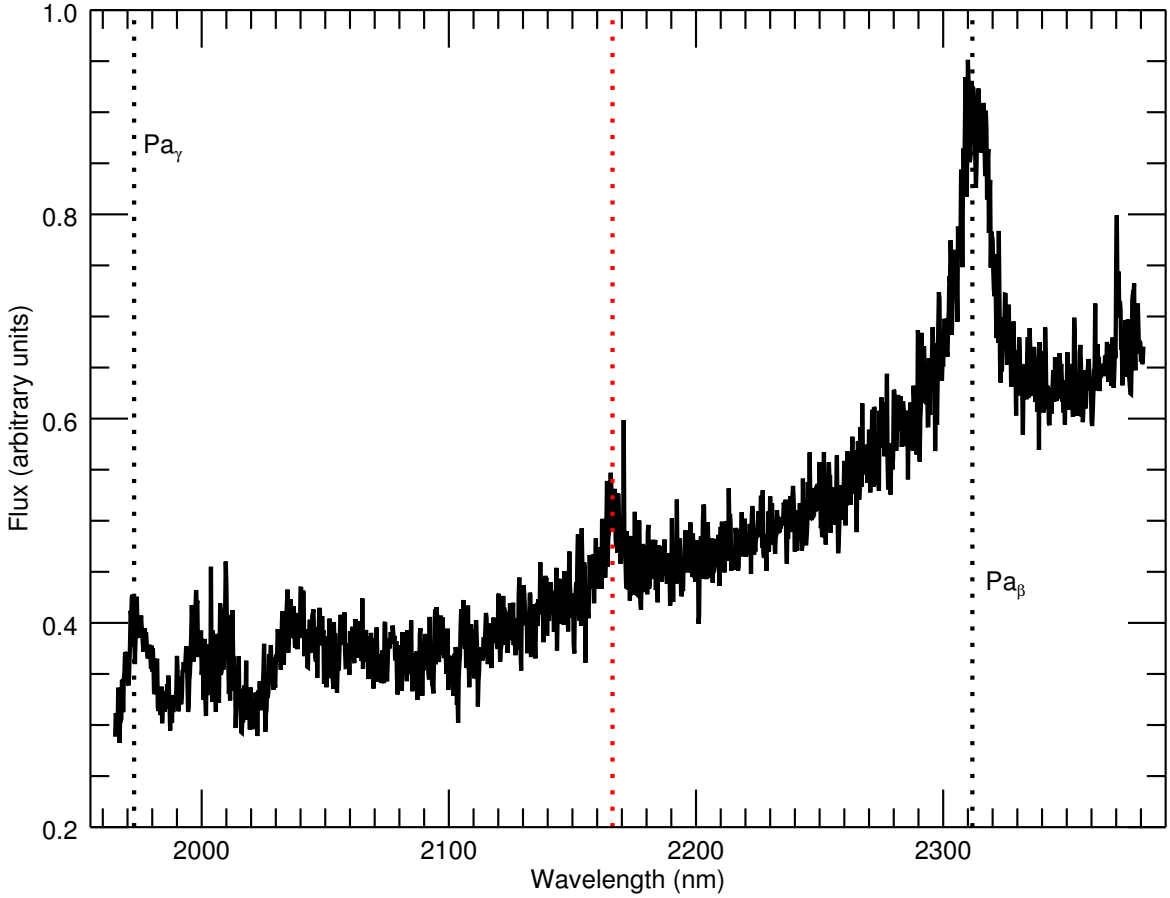

Fig. 4.3. Emission spectrum of F2M0825+4716. Black vertical dotted lines denote redshifted wavelengths corresponding to the Paschen energy transitions of hydrogen, Pa$_\gamma$ (rest wavelength 1094.1 nm) and Pa$_\beta$ (1282.2 nm). The red dotted line represents the emission line (∼1200 nm) from an unknown element. The redshift of this source is $z = 0.801$. Absorption lines in the first part of the graph are either residuals from the telluric correction, or absorption lines of the host galaxy.

To further investigate the kinematics of F2M0825+4716, we extract the emission spectrum over the spatial spread of the host galaxy. The spectrum is populated with dominant broad emission lines suggesting the quasar's activity. Figure 4.3 shows the host galaxy's emission spectrum for F2M0825+4716. We identify clear Pa$_\gamma$ (rest wavelength 1094.1 nm) and Pa$_\beta$ (1282.2 nm). At a rest wavelength of approximately 1200 nm, another broad emission line is

detected. NIST's database [17] provides several elements corresponding to the given energy transition. However, none of the NIST-identified transitions are reported as common in spectral templates for quasars [18], leaving one of the F2M0825+4716's emission peaks unidentified. It is important to note that a strong 1200-nm emission line is present in every spectrum extracted from each pixel within the bright region, eliminating the possibility of a glitch or a cosmic ray.

4.2 F2345-1003

Observations of F2345-1003 source were conducted on November 6^{th}, 2012. The filter used throughout was Hbb, allowing for a range in wavelength from 1473 nm to 1803 nm. The Hbb transition curve is shown in Fig. 4.4. The observations were operated using the spatial scale employed of 0.1 arcsec, providing a field of view of 1.6×6.4 arcsec^2. The integration time used to observe the source was 600 s. A total of 120 min of the target observation, and 50 min of the sky observation were accomplished. A close-by NGS was observed for 20 s, providing the necessary frames for the telluric (atmospheric) correction.

Figure 4.1(b) shows the final three-dimensional data cube for F2345-1003. Analogously to the previously conducted analysis of the F2M0825+4716 source, we approximate the angular size of the host galaxy to be $\theta = 1.9$ arcsec (19 pixels). With the redshift $z = 0.263$ and the current cosmological parameters, we find that the angular size distance D_A is 844 Mpc [12], concluding that the observed linear size of the host galaxy is 7.8 kpc. Among the objects observed, F2345-1003 is the closest.

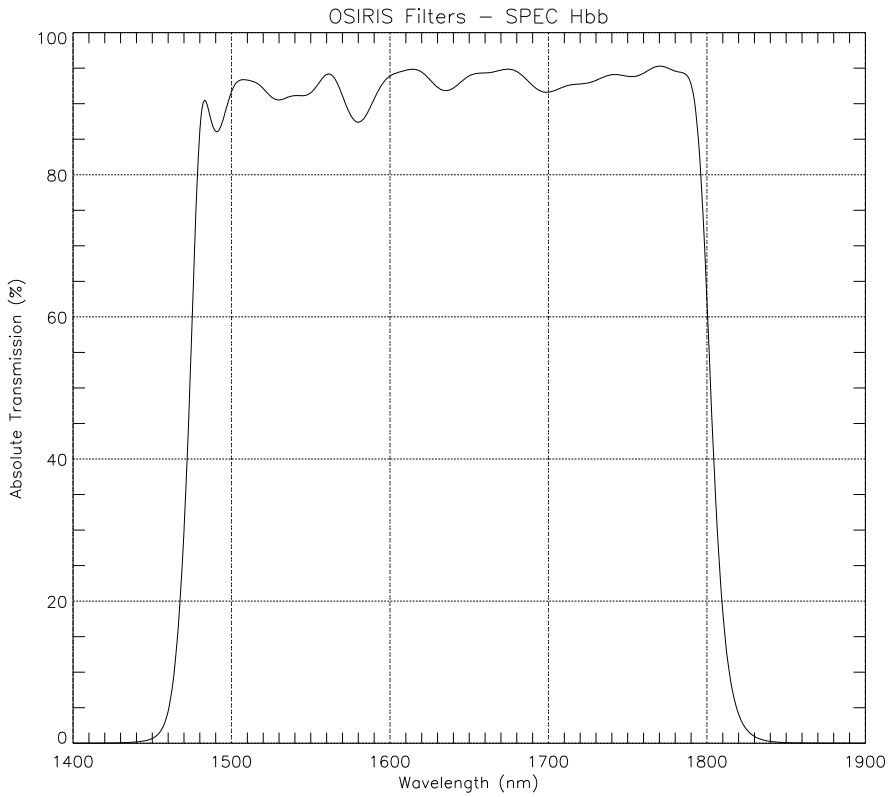

Fig. 4.4. Transmission curve for the H-band Hbb filter, used for the observation of F2345-1003, allowing the transmission range from 1473 nm to 1803 nm.

Fitting a Gaussian to the extended bright region results in a FWHM of 8.45 pixels ($\sim$3.46 kpc) in the horizontal direction, and 5.67 pixels ($\sim$2.32 kpc) in the vertical direction. This asymmetry may be suggestive of a significant degree of merger activity, or indicative of an edge-on view of a galactic disk. To probe further into the characteristics of the host galaxy, we extract its emission spectrum shown in Fig. 4.5.

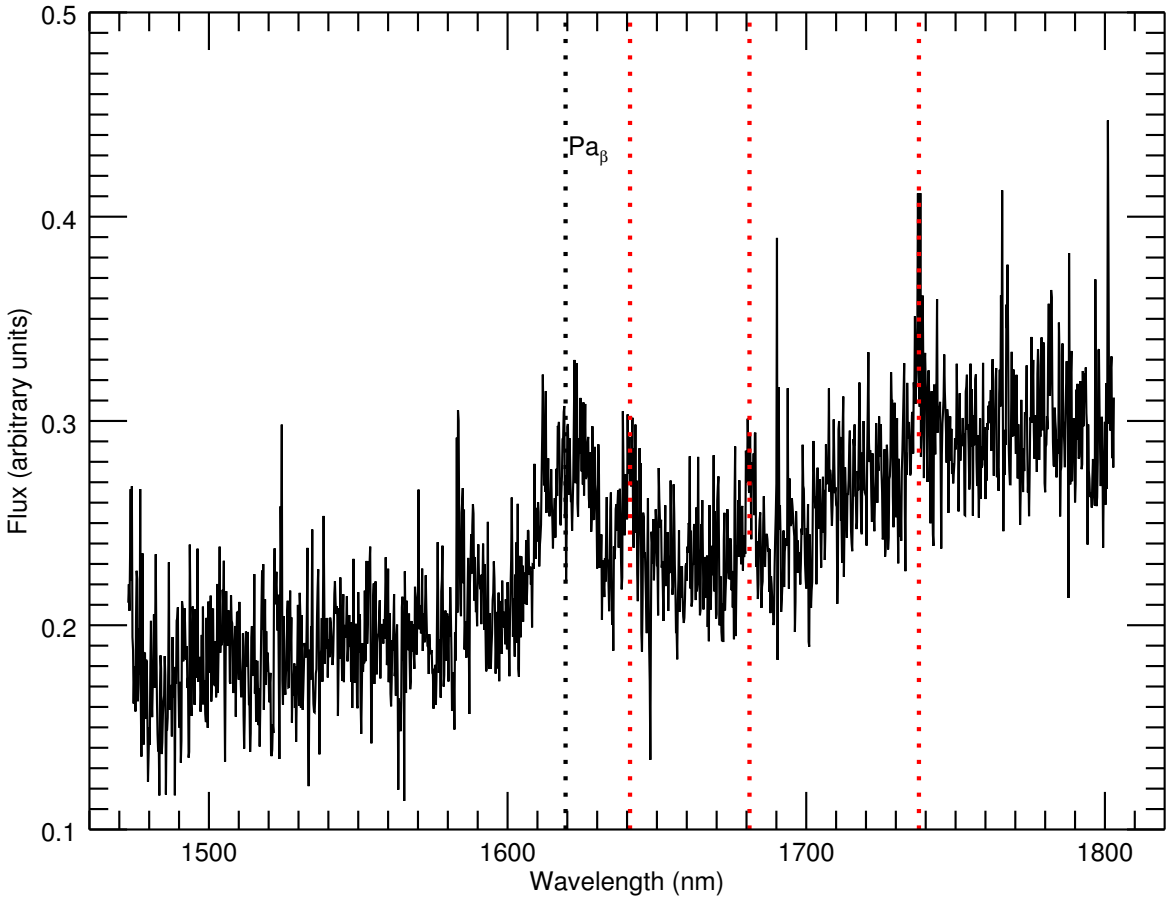

Fig. 4.5. Emission spectrum of F2345-1003. The black vertical dotted line represents redshifted wavelength corresponding to energy transitions of Pa$_\beta$ (1282.2 nm). In red are broad transition lines from unknown elements, corresponding to rest wavelengths of approximately 1300 nm, 1330 nm, and 1375 nm. The redshift of this source is $z = 0.263$. Note the double-peaked line profile of Pa$_\beta$ emission line, suggesting unusual kinematic/velocity structure of the source.

Similarly to the preceding source, we detect emission lines at wavelengths not previously reported in the literature [18]. Comparing the shape of the Pa$_\beta$ emission line in Fig. 4.5 to the one in Fig. 4.3, we observe that instead of a single-peaked high-amplitude line profile, the signal of Pa$_\beta$ in Fig. 4.5 is weak and shows splitting. This feature is prominent throughout the entire bright region, changing ever-so-slightly and it may be suggestive of possible unusual kinematic taking place in the source.

4.3 S82M2226-0032

The optical spectrum of S82M2226-0032 contains emission lines uncharacteristic of any known astrophysical source [1]. Figure 4.6 shows SDSS's spectrum with a high-signal broad [Mg II] emission line, as well as a weak [O III] line, both indicators of an atypical AGN. Its unusual features in the optical region were one of the determining factors in choosing S82M2226-0032 as our target.

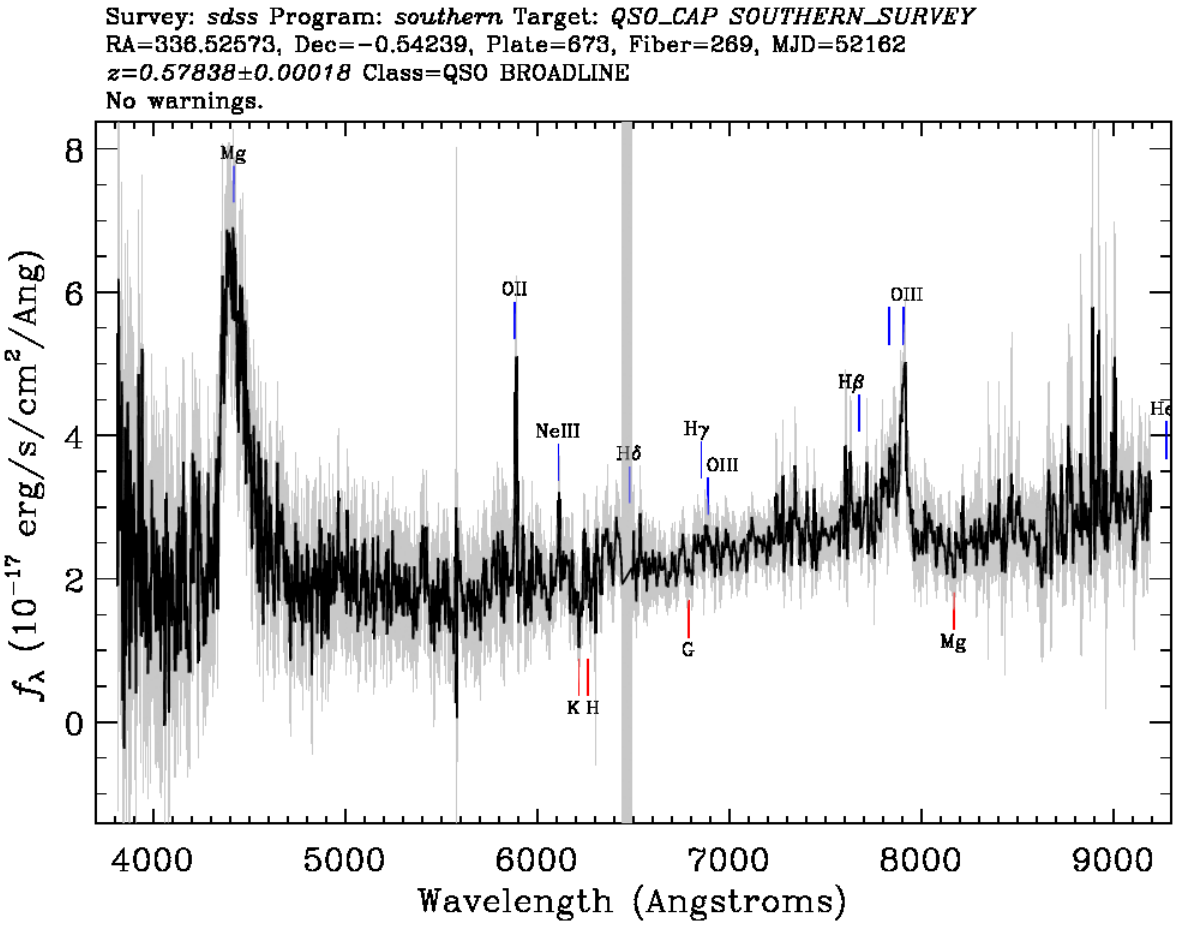

Fig. 4.6. Optical spectrum of S82M2226-0032. A strong [Mg II] emission line and a weak [O III] make this source unusual. Credits: SDSS

Observations of the S82M2226-0032 source were conducted on November 5$^{\text{th}}$, 2012. The filter used for the observations was Zbb, allowing the transition range from 999 nm to 1176 nm [13]. Similarly to previous observations, a spatial scale of 0.1 arcsec was employed, providing a

field of view of 1.6×6.4 arcsec^2. An integration time of 900 s was used to observe the source, resulting in a total of 105 min of the target, and 45 min of the sky observation. A close-by NGS is observed for 20 s.

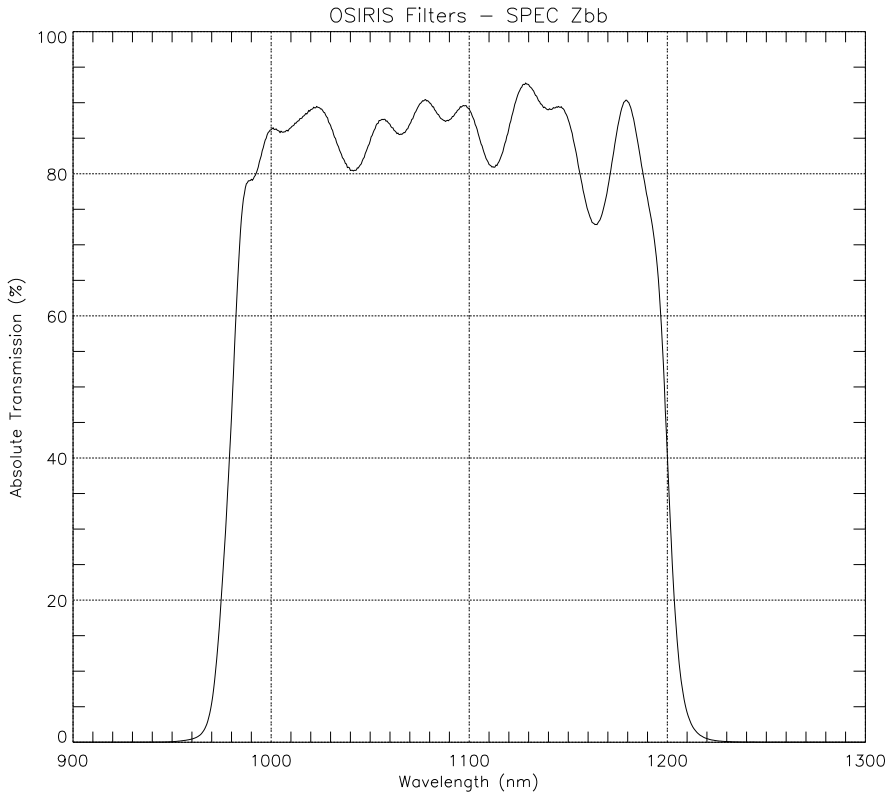

Fig. 4.7. Transmission curve for the z-band Zbb filter, used for the observation of S82M2226-0032, allowing the transmission range from 999 nm to 1176 nm.

The S82M2226-0032 mosaicked cube is shown in Fig. 4.1(c). The redshift of the source $z = 0.578$ implies an angular size distance of $D_A = 1370.2$ Mpc [12]. Approximating the angular size to 0.8 arcsec (8 pixels) results in a linear size of 5.3 kpc. Furthermore, fitting a Gaussian to the bright region concludes in a FWHM of 2.58 pixels (∼1.71 kpc) in the horizontal, and only 0.17 pixels (∼0.11 kpc) in the vertical direction. Again, this large asymmetry combined with the optical image from SDSS suggests a dynamical system, or an edge-on view.

Similarly to the optical information, the near-infrared emission spectrum from the bright

region in S82M2226-0032 contains unusual emission lines. We identify H_α (656.3 nm), N II (658.3 nm), and S II (673.1 nm), whilst lines at rest wavelengths of ∼637 nm and ∼694 nm remain unidentified. The emission spectrum of S82M2226-0032 is shown in Fig. 4.8.

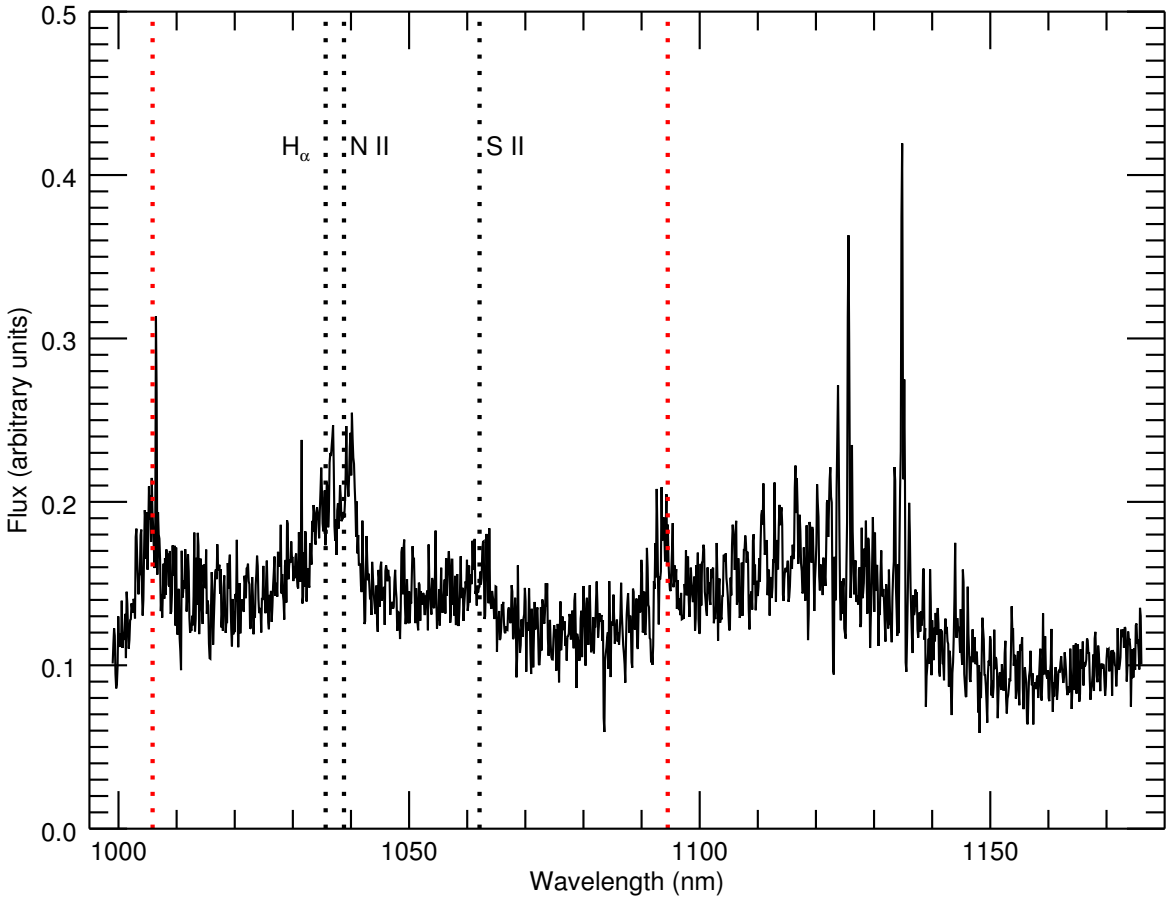

Fig. 4.8. Emission spectrum of S82M2226-0032. Black vertical dotted lines represent redshifted wavelengths corresponding to transitions of H_α (656.3 nm), N II (658.3 nm), and S II (673.1 nm). The red lines corresponding to rest wavelengths of ∼637 nm and ∼694 nm remain unknown. The redshift of this source is $z = 0.578$. Strong peaks following the O II emission are emission lines from the sky.

5 Conclusions and future research

In this project we successfully reduced and analyzed the OSIRIS+AO data for three out of five observed sources. The main focus was on performing the data reduction using the OSIRIS pipeline. Since the function of the pipeline has been proven, the reduction of the remaining two sources should be less time-consuming. Once reduced, the spectra of three sources were carefully analyzed. Results are summarized in Table 5.1

Table 5.1. Summary of the results for three reduced sources.

Object	z	Linear size	FWHM		Emission lines	
			horizontal	vertical	known	unknown
		(kpc)	(kpc)	(kpc)	rest, (nm)	observed, (nm)
F2M0825+4716	0.803	13	1.19	1.17	1094.1, 1282.2	2164
F2345-1003	0.263	7.8	3.46	2.32	1282.2	1641, 1680, 1738
S82M2226-0032	0.578	5.3	1.71	0.11	656.3, 658.3, 673.1	1005, 1095

We identified broad emission lines from quasars, but no apparent narrow star formation lines are evident from the spectra obtained, thus no conclusive results with regards to the correlation between star-forming rates and quasar's activity can be stated at this point. The first step towards computing star formation rates for each source is the flux calibration published in [13]. Subtracting the spectrum of a quasar from that of its host galaxy would hopefully leave behind emission lines from star-forming regions, allowing further analysis.

Furthermore, the spectral resolution of the OSIRIS instrument can be further utilized to create spatially resolved velocity maps for each source. To do so, each pixel in a data cube should be considered separately, and detailed analysis of its spectrum should be performed. Creating

velocity maps will provide a detailed insight into the kinematics of each source.

To address the question of the unusual emission lines identified in our sources, one can perform Gaussian fitting to find their corresponding energies. This will allow for an investigation about the type or relative spatial orientation of an astrophysical object required to fuel such emission. In turn, this analysis may provide us with more information about the orientation of the quasar, or indicate a presence of some other energetic sources close-by.

Finally, an interesting investigation that would further characterize observed sources would be overlapping the near-infrared images used in this project with already existent optical data from SDSS or HST. This would create a more complete picture of our sources over a wider range of wavelengths. We would expect to see comparable brightnesses of the quasar in these two near-by regions of the electromagnetic spectrum.

Bibliography

[1] D. E. Osterbrock. *Astrophysics of Gaseous Nebulae and Active Galactic Nuclei.* University Science Books, 1989.

[2] K. I. Kellermann. The Discovery of Quasars and its Aftermath. *Journal of Astronomical History and Heritage*, pages 267–282, March 2014.

[3] K. I. Kellermann, R. Sramek, M. Schmidt, D. B. Shaffer, and R. Green. VLA observations of objects in the Palomar Bright Quasar Survey. *The Astronomical Journal*, 98:1195–1207, October 1989.

[4] R. Barnett, S. J. Warren, M. Banerji, R. G. McMahon, P. C. Hewett, D. J. Mortlock, C. Simpson, B. P. Venemans, K. Ota, and T. Shibuya. The spectral energy distribution of the redshift 7.1 quasar ULAS J1120+0641. *Astronomy and Astrophysics*, March 2015.

[5] T. C. Urrutia. *Discovery and analysis of dust-reddened type I quasars – Finding the missing link in quasar evolution.* Thesis Dissertation. University of California, Davis, February 2008.

[6] E. Glikman, B. Simmons, M. Mailly, K.Schawinski, C. M. Urry, and M. Lacy. Major mergers host the most luminous red quasars at z $\sim$ 2: A Hubble Space Telescope WFC3/IR Study. *The Astrophysical Journal*, June 2015.

[7] P. F. Hopkins, L. Hernquist, T. J. Cox, and D. Keres. A cosmological framework for the co-evolution of quasars, supermassive black holes, and elliptical galaxies: I. galaxy mergers quasar activity. *The Astrophysical Journal*, June 2007.

[8] E. Glikman. Probing Quasar/Galaxy Co-Evolution: Integral Field Spectroscopy of Dust-Obscured Quasars. *Yale University Proposal*, March 2012.

[9] D. B. Sanders, B. T. Soifer, J. H. Elias, B. F. Madore, K. Matthews, G. Neugebauer, and N. Z. Scoville. Ultraluminous infrared galaxies and the origin of quasars. *The Astrophysical Journal*, pages 74–91, February 1988.

[10] M. Schmidt. The Rate of Star Formation. *The Astrophysical Journal*, page 243, March 1959.

[11] H. Cullen, P. Alexander, D. A. Green, M. Clemens, and K. Sheth. The unusual distribution of molecular gas and star formation in Arp 140. *Monthly Notices of the Royal Astronomical Society*, June 2006.

[12] N. Wright. *A Cosmology Calculator for the World Wide Web*. Available at http://www.astro.ucla.edu/wright/CosmoCalc.html (accessed Dec 2016). Department of Astronomy, UCLA.

[13] J. Larkin, M. Barczys, M. McElwain, M. Perrin, J. Weiss, and S. Wright. OSIRIS Users' Manual. *UCLA Infrared Laboratory*, 2010.

[14] R. A. Freedman, R. M. Geller, and W. J. Kaufmann III. *Universe*. W. H. Freeman and Company, 2011.

[15] J. Allington-Smith, R. Content, R. Haynes, and D. Robertson. Integral field spectroscopy with GEMINI and Space Telecopes. *Imaging the Universe in Three Dimensions. Proceedings from ASP Conference Vol. 195. Edited by W. van Breugel and J. Bland-Hawthorn.*, 2000.

[16] M. Najarian. Using Integral-Field Spectroscopy of Dust Obscured Quasars to Probe Quasar/Galaxy Co-Evolution. *Senior Project report, Middlebury College*, May 2014.

[17] A Kramida, Yu. Ralchenko, and J. Reader. *NIST Atomic Spectra Database*. ([Online.] Available: http://physics..gov/asd (accessed December 2016). National Institute of Standards and Technology, Gaithersburg, MD., 2015.

[18] E. Glikman, D. J. Helfand, and R. L. White. A near-infrared spectral template for quasars. *The Astrophysical Journal*, November.